SCIENTIFIC REPORTS

OPEN

SUBJECT AREAS:
NANOTECHNOLOGY IN CANCER
NANOPARTICLES

Received
20 January 2014

Accepted
25 February 2014

Published
28 March 2014

Correspondence and requests for materials should be addressed to Q.L. (liquan@phy.cuhk.edu.hk)

Unambiguous observation of shape effects on cellular fate of nanoparticles

Zhiqin Chu[1], Silu Zhang[1], Bokai Zhang[1], Chunyuan Zhang[2], Chia-Yi Fang[3], Ivan Rehor[4], Petr Cigler[4], Huan-Cheng Chang[3], Ge Lin[2], Renbao Liu[1,5] & Quan Li[1,5]

[1]Department of Physics and Centre for Quantum Coherence, The Chinese University of Hong Kong, Shatin, New Territories, Hong Kong, [2]School of Biomedical Sciences, Faculty of medicine, The Chinese University of Hong Kong, Shatin, New Territories, Hong Kong, [3]Institute of Atomic and Molecular Sciences, Academia Sinica, Taipei 106, Taiwan, [4]Laboratory of Synthetic Nanochemistry, Institute of Organic Chemistry and Biochemistry AS CR, v.v.i., Flemingovo nam. 2, 166 10, Prague 6, Czech Republic, [5]The Chinese University of Hong Kong ShenZhen Research Institute, ShenZhen, China.

Cellular fate of nanoparticles is vital to application of nanoparticles to cell imaging, bio-sensing, drug delivery, suppression of drug resistance, gene delivery, and cytotoxicity analysis. However, the current studies on cellular fate of nanoparticles have been controversial due to complications of interplay between many possible factors. By well-controlled experiments, we demonstrated unambiguously that the morphology of nanoparticles independently determined their cellular fate. We found that nanoparticles with sharp shapes, regardless of their surface chemistry, size, or composition, could pierce the membranes of endosomes that carried them into the cells and escape to the cytoplasm, which in turn significantly reduced the cellular excretion rate of the nanoparticles. Such features of sharp-shaped nanoparticles are essential for drug delivery, gene delivery, subcellular targeting, and long-term tracking. This work opens up a controllable, purely geometrical and hence safe, degree of freedom for manipulating nanoparticle-cell interaction, with numerous applications in medicine, bio-imaging, and bio-sensing.

The cellular fate of nanoparticles (NPs), i.e., their intracellular translocation after cellular uptake and their final destiny, is relevant not only to their cytotoxicity[1,2], but also to NP-based drug delivery[3,4], gene delivery[5,6], long term tracking[7,8], and bio-sensing[9,10]. While a large amount of research work has been devoted to studying endocytosis (a major route of NPs' cellular uptake[11–14]), only limited understanding has been obtained on NPs' cellular fate after they enter the cells. Right after endocytosis the NPs reside in membrane-bounded vesicles[11,15] (i.e., endosomes, which would evolve into lysosomes or autophagosomes[16,17] at a later stage). The intracellular translocation largely depends on whether the NPs can escape from the endosomes, and so does the NPs' final destiny. Whether or not the NPs can escape into cytoplasm before the endosomes mature into lysosomes is critical to the efficacy of NP-assisted delivery of drugs[4], DNA[18], siRNA[19], or protein[20]. Therefore it is highly desirable to understand and control the trespass processes of NPs across the endosomal membranes.

However, the study of cellular fate of NPs has been complicated by interplay of various chemical and electrostatic interactions between NPs and the lipid bilayer membranes of endosomes. Some studies showed the importance of the surface composition[21–25] and charge[3,26,27]. Other recent studies revealed the effects of NPs' aspect ratios[28] on NP-membrane interaction, which allude to the relevance of morphology in membrane penetration of NPs. The discovery of cell penetration of sharp-edged graphene[29] also indicated the role of morphology. These apparently contradicting observations, together with the difficulty in excluding the interplay of various chemical, electrostatic, and morphological factors by control experiments, make the mechanisms of NPs' cellular fate an open question.

In this study, we unambiguously demonstrated the role of the morphological features in determining the cellular translocation dynamics and fate of NPs by a series of control experiments. We employed well controlled surface modification to separate the morphological effects from the surface composition and charge effects (Fig. 1). In particular, we found NPs with sharp corners and edges could easily break the endosomal membranes and in turn reside in cytoplasm for a long time without being excreted, regardless of their surface compositions, charges, materials, and sizes. In contrast, spherical NPs have distinctively different cellular dynamics: they stably remain in endosomes after endocytosis, evolve with endosome maturation, and can be easily excreted via exocytosis[30]. This discovery of the morphological effects on NPs' cellular fate opens up a controllable, purely geometrical and hence safe, approach to manipulating NP-cell interactions, which are useful for many applications such as NP-assisted drug delivery and long term tracking.

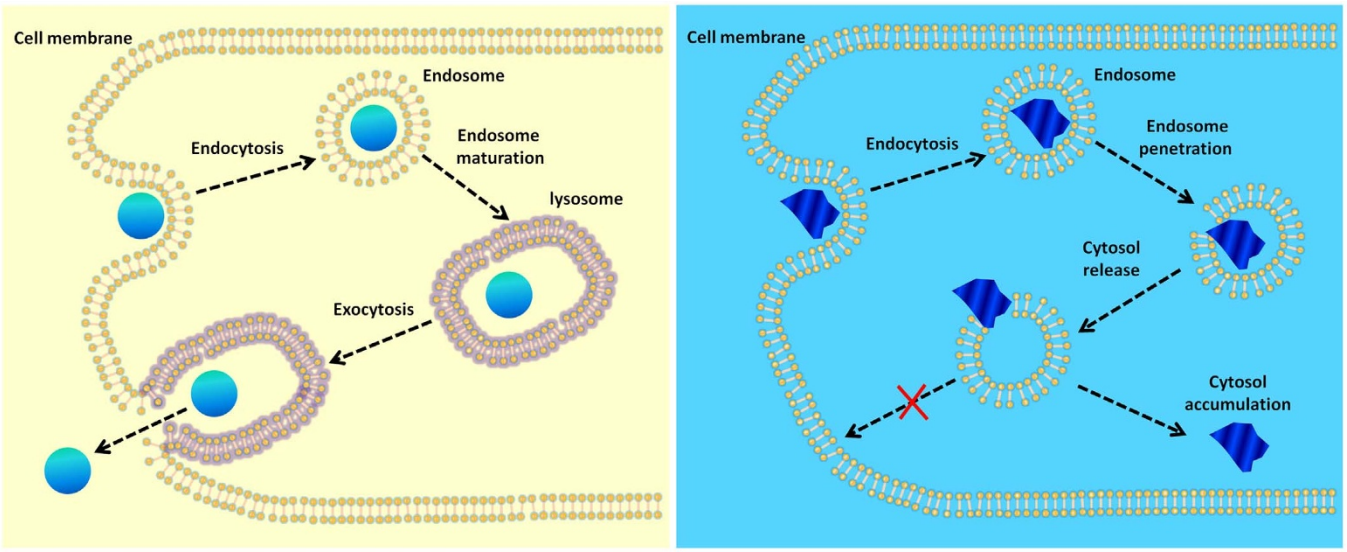

Figure 1 | Schematics of intracellular trafficking of nanoparticles with different morphological features. Left: A nanoparticle with low sharpness enters the cell via endocytosis with the endosome as the vehicle, stably resides in the endosome, which evolves into the lysosome by endosomal maturation, and finally exits the cell via exocytosis with the lysosome as the vehicle. Right: A sharp-shaped nanoparticle enters the cell via endocytosis with the endosome as the vehicle and escapes the endosome by rupturing the endosomal membrane before the lysosome is formed. Without a lysosome as the vehicle, the nanoparticle has very low excretion rate and will stay in the cytoplasm for a long time.

Results

We started with the investigation of nanodiamonds (NDs) that had irregular shapes with sharp corners. We found that such NDs escaped from endosome to cytoplasm shortly (a couple of hours on average) after their cellular uptake, and could hardly exit the cells afterwards. These characteristics were completely opposite to those of spherical SiO_2 NPs (which resided in endosome or lysosome as long as for days and had easy cellular excretion). Then we carried out experiments that independently modified the surface composition and morphology of the NDs, and examined the intracellular translocation of the modified NPs. The round-shaped NDs had cellular dynamics similar to that of SiO_2 NPs; the sharp-shaped NDs coated with thin layers of SiO_2 behaved similarly to uncoated sharp-shaped NDs. These results evidenced the critical role of NPs' morphology in their intracellular trafficking. Such a mechanism was further confirmed by studying the cellular fate of Au NPs with different morphological features, which had completely different surface chemistry and electrostatic characteristics from those of NDs or SiO_2. We further established the correlation between the intracellular translocation behavior and the cellular excretion of NPs, that is, the NPs that pricked the endosomal membranes tended to stably retain in cytoplasm with difficult cellular excretion.

Surprising intracellular dynamics and low excretion rate of nanodiamonds. We employed fluorescent NDs with a physical size distribution of tens to hundreds of nanometers (Supplementary Fig. S1a). The aspect ratio of these crystalline particles was close to 1. They had irregular shapes and most of them had at least 1–2 sharp corners (Fig. 2a). The NDs' average hydrodynamic radius, which reflected their averaged ensemble size (representing the "actual size" during NDs-cell interactions) when dispersed in aqueous solutions (Phosphate buffered saline (PBS) buffer in current study), was determined as ~115 nm (Supplementary Fig. S2) by dynamic light scattering. Fourier transform infrared spectroscopy (FTIR) spectrum (Fig. 2b) of the NDs showed a peak at 1780 cm^{-1}, which is characteristic of the C = O bonds, suggesting the predominance of −COOH on the NDs' surfaces[31]. The surfaces of such NDs were negatively charged, with zeta potential measured as −28 mV at pH ~ 7.6 (Supplementary Fig. S3). The nitrogen-vacancy (NV) centers in the NDs gave a strong fluorescence peak at ~680 nm under excitation at 514 nm (Supplementary Fig. S4), which we utilized for NDs tracking in the in vitro experiments.

NDs were found to enter cells easily (Supplementary Fig. S5), and endocytosis was identified as the major cellular uptaken mechanism (Supplementary Fig. S6). Shortly after their cellular entry, the NDs escaped from the endosomes and were translocated to cytoplasm. After a long duration of incubation, the NDs were found mostly outside the endosomes (overlap coefficient of NDs with endosome markers gradually decreased from ~0.8 (1 hour) to ~0.1 (8 hours), as shown in Fig. 2c–g & 2m). The NDs only resided in early endosomes, and they seldom had chance to be translocated to late endosome or lysosome, before they escaped to the cytoplasm (overlap coefficient of NDs with lysotracker remained ~0.2 for all durations of incubation, as shown in Fig. 2h–l & 2m).

Transmission electron microscopy (TEM) observations also confirmed that the NDs entered the cells via endocytosis and escaped the endosomes to cytoplasm. TEM micrographs were taken for tens of cell samples incubated with NDs for 24 hours to find the intracellular localization of the NDs. For such a long incubation time, NDs were occasionally observed in membrane-bounded vesicles (Fig. 2n), but a majority of them were found in cytoplasm (TEM images in Fig. 2o–q). In fact, some of the NDs were found in the process of "penetrating" the membranes of a vesicle (Fig. 2q). In addition, confocal microscopy and TEM results showing similar NDs' intracellular translocation behaviors were also obtained in other cell lines examined. The only difference was the time scale of ND's endosomal escape (Supplementary Fig. S7 and Fig. S8).

Then we investigated excretion of the NDs. After incubation with NDs for 12 hours, the cells were transferred to NDs-free culture medium and incubated for another 12 hours. Confocal microscopy images taken after the first 12 hours' incubation showed that the NDs had entered the cell interiors (Fig. 2r & s). Further incubation in NDs-free medium resulted in negligible percentage of NDs "washed out" from the cells (Fig. 2t & u). The low excretion rate of NDs was further confirmed by quantitative flow-cytometry data (Supplementary Fig. S9). These results suggested correlation between the cellular translocation and the excretion of the NPs. It has been known that the usual route of NPs' cellular excretion is via exocytosis—a reverse process of endocytosis[30,32]. This process is assisted by membrane-bounded vesicles[30,33]. When the NPs escaped to the

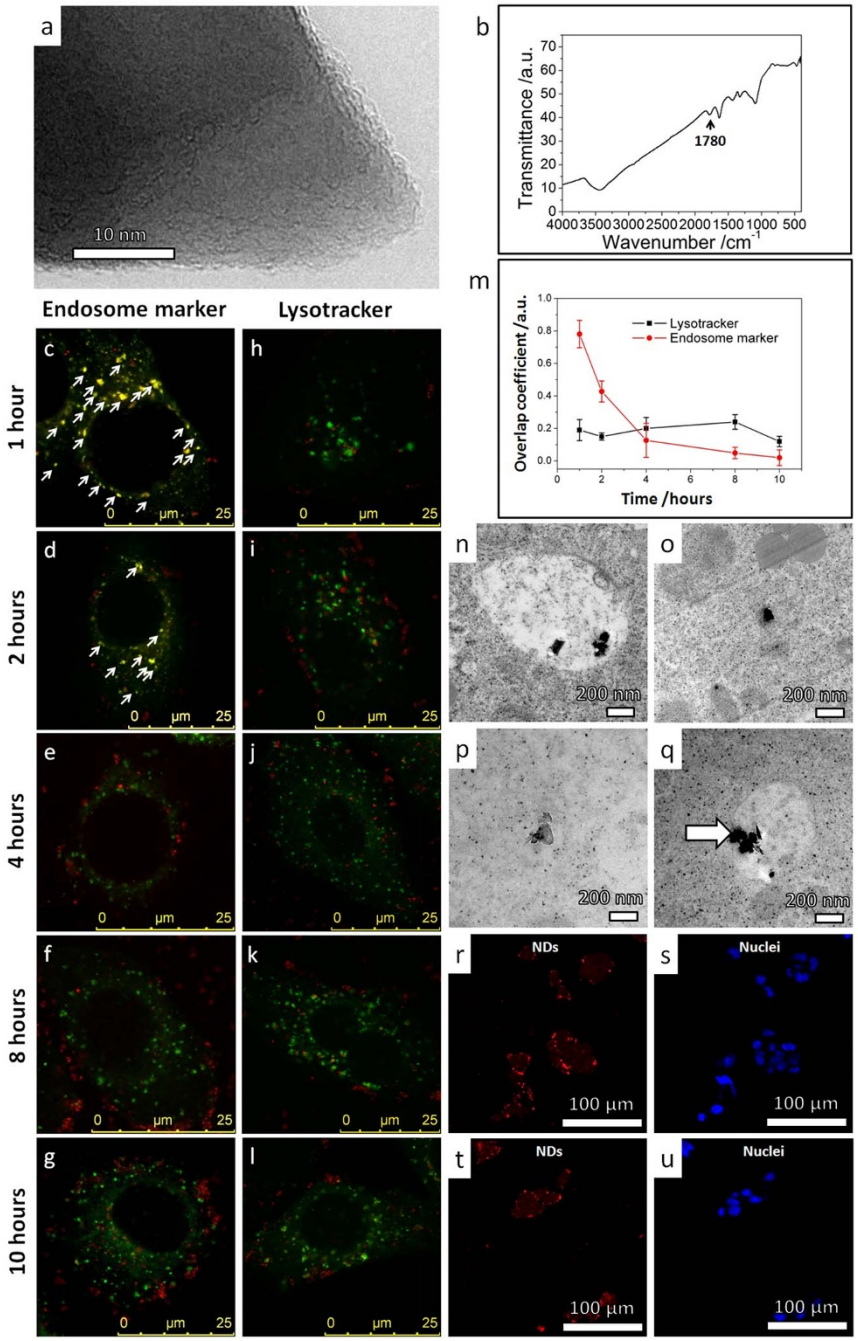

Figure 2 | Intracellular translocation of sharp-shaped nanodiamonds from membrane bounded vesicles and stable residence in cytoplasm. (a) High resolution TEM image showing the sharp corner of a typical nanodiamond. (b) FTIR spectrum of the nanodiamonds showing a characteristic dip (1780 cm^{-1}) of a −COOH rich termination surface. (c–g) Representative confocal microscopy images showing the fluorescent signals of endosome markers (green) and nanodiamonds (red) in HepG2 cells after cell incubation with nanodiamonds in serum-free medium for (c) 1 hour, (d) 2 hours, (e) 4 hours, (f) 8 hours and (g) 10 hours. The yellow spots show spatial overlap between nanodiamonds and endosomes (as marked by white arrows). The observed low overlap for longer incubation durations indicates that the nanodiamonds escaped the endosomes. (h–l) Representative confocal microscopy images showing the fluorescent signals of lysotracker (green) and nanodiamonds (red) in HepG2 cells after cell incubation with nanodiamonds in serum-free medium for (h) 1 hour, (i) 2 hours, (j) 4 hours, (k) 8 hours and (l) 10 hours. Very low spatial overlap between nanodiamonds and lysosomes was observed, indicating that most nanodiamonds escaped the endosomes before the lysosomes were formed. (m) The overlap coefficients of nanodiamonds with endosomes (red symbols) or lysosomes (black symbols) functions of the incubation duration. (n–q) TEM images showing the typical intracellular distribution of nanodiamonds in HepG2 cells after incubation in serum-free medium for 24 hours: (n) TEM image of nanodiamonds residing in a membrane-bounded vesicle; (o, p) TEM images of nanodiamonds in the cytoplasm (majority); (q) TEM image of nanodiamonds piercing the membrane of a vesicle. (r–u) Representative confocal microscopy images showing the uptake and excretion of nanodiamonds in HepG2 cells as revealed by the fluorescence of nanodiamonds (red). The nuclei were stained by DAPI (blue). (r,s) HepG2 cells were incubated with nanodiamonds in serum-free medium for 12 hours. Punctated red dots show effective cellular uptake of nanodiamonds. (t,u) HepG2 cells were incubated for additional 12 hours in serum-free medium without nanodiamonds. The punctated-red-dot pattern remains unchanged, suggesting that most nanodiamonds remained in cells without being "washed out".

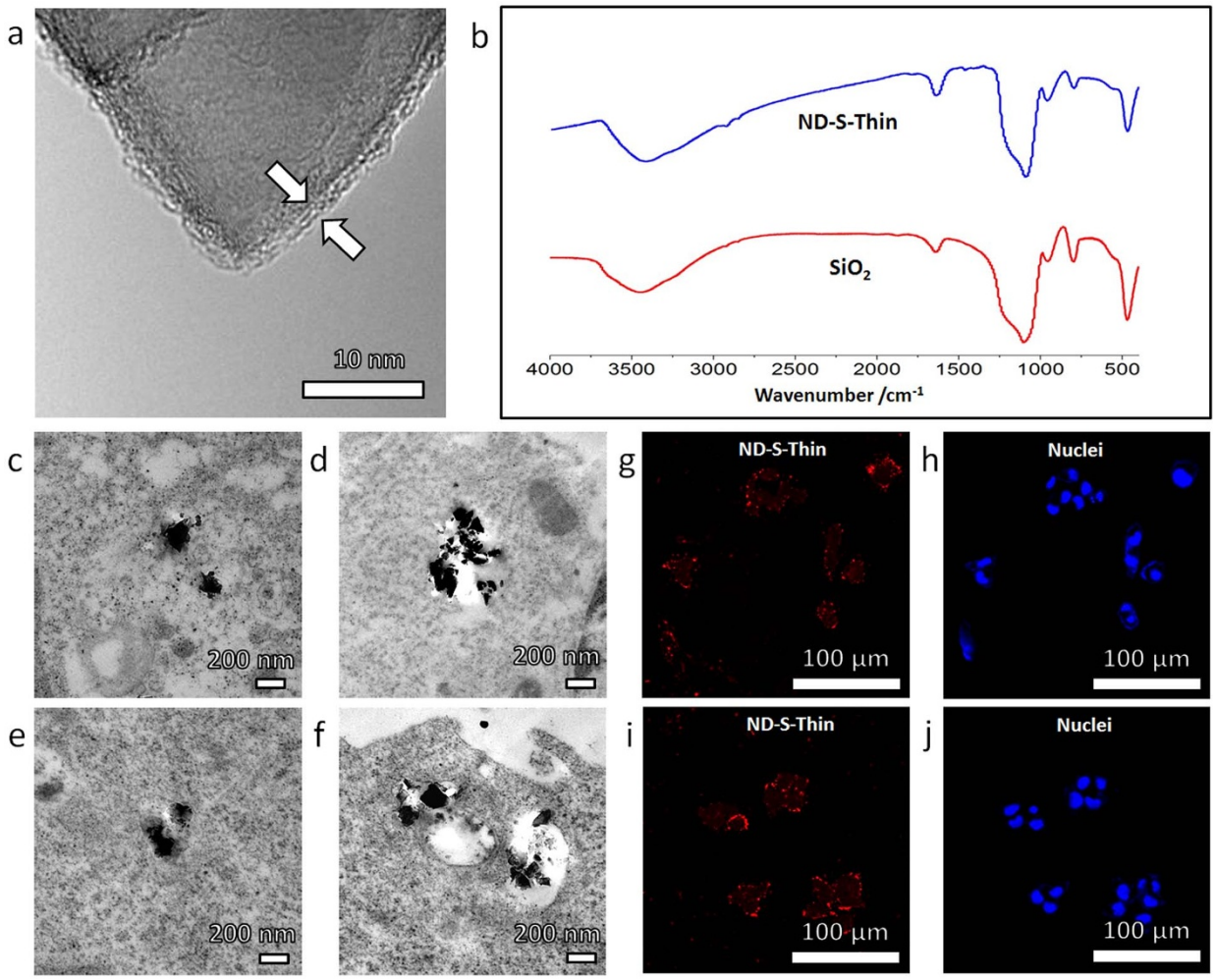

Figure 3 | Intracellular translocation and excretion behaviors of (ND-S-Thin) particles (nanodiamonds coated with thin layers of SiO_2). The cellular dynamics of ND-S-Thin was observed similar to that of uncoated nanodiamonds (as shown in Fig. 2). (a) High-resolution TEM image showing a ~2 nm silica shell on the surface of a ND-S-Thin particle, with morphology similar to uncoated nanodiamonds. (b) Similarity between FTIR spectra of ND-S-Thin and SiO_2 particles indicates that the two kinds of nanoparticles have similar surface chemistry. (c–f) TEM images showing the typical distribution of ND-S-Thin particles in HepG2 cells after incubation in serum-free medium for 24 hours: (c–e) TEM images of ND-S-Thin particles in cytoplasm; (f) TEM image of ND-S-Thin particles penetrating the membrane of the vesicle. (g–j) Representative confocal microscopy images showing the uptake and excretion of ND-S-Thin particles in HepG2 cells as revealed by the fluorescence of nanodiamonds (red). The nuclei were stained by DAPI (blue). (g,h) HepG2 cells were incubated for 12 hours in serum-free medium with ND-S-Thin particles. Punctated red dots show effective cellular uptake. (i,j) HepG2 cells were incubated for additional 12 hours in nanoparticle-free serum-free medium. The punctated-red-dot pattern remains unchanged, suggesting that most ND-S-Thin particles remained in cells without being "washed out".

cytoplasm as in the case of NDs in our experiments, their motion became difficult. This was supported by the movement tracking experiments of NDs inside live cells after 24 hours' incubation (Supplementary Fig. S10). Most of the NDs, tracked for tens of minutes inside cells, had small displacement (~1000 nm). The mean velocity of NDs was estimated at ~ tens of nm/second, which was two orders of magnitude lower than the typical velocity (~1 μm/second) of molecular motors inside cells[34]. All tracked NDs presented the "pearls-on-a-string" trajectories, which are characteristic of immobile objective[33]. Immobilization reduced the probability for the NDs to approach the plasma membrane, which is a prerequisite for exocytosis or direct penetration to occur. Therefore the cellular excretion rate was significantly suppressed.

The characteristics of cellular translocation and excretion of NDs were completely different from those of amorphous SiO_2 NPs (Supplementary Fig. S11). The cellular uptake of SiO_2 via endocytosis has been well documented in literature[35]. Once inside the cells, they stably resided in endosome or lysosome, and were seldom found in cytoplasm (Supplementary Fig. S12). In addition, almost all of the uptaken SiO_2 NPs were "washed out" from the cells under similar experimental conditions (Supplementary Fig. S13). We notice that the NDs had sharp corners and edges, in contrast to the round-shape of SiO_2 NPs used in previous experiments (Supplementary Fig. S11). While the observations suggested the role of the morphological features of NPs, other factors such as the surface chemistry, surface charge, and size of NPs have not been excluded yet. In our previous study, SiO_2 NPs with size ranging from 40–400 nm had been tested, and no size effects were observed[35,36].

Exclusion of the effects of surface chemistry and electrostatics. To investigate the effect of the surface characteristics, we coated NDs with thin layers of SiO_2 (Sample ND-S-Thin). These ND-S-Thin particles have the same morphological feature and size as uncoated NDs (Supplementary Fig. S1b). The average hydrodynamic radius of the NPs in such a sample was ~121 nm, similar to that of the uncoated NDs (Supplementary Fig. S2). The thickness of the SiO_2 layer was ~2 nm (inset of Fig. 3a). XPS spectra taken from such a sample showed characteristic signals of Si and O, as originated from

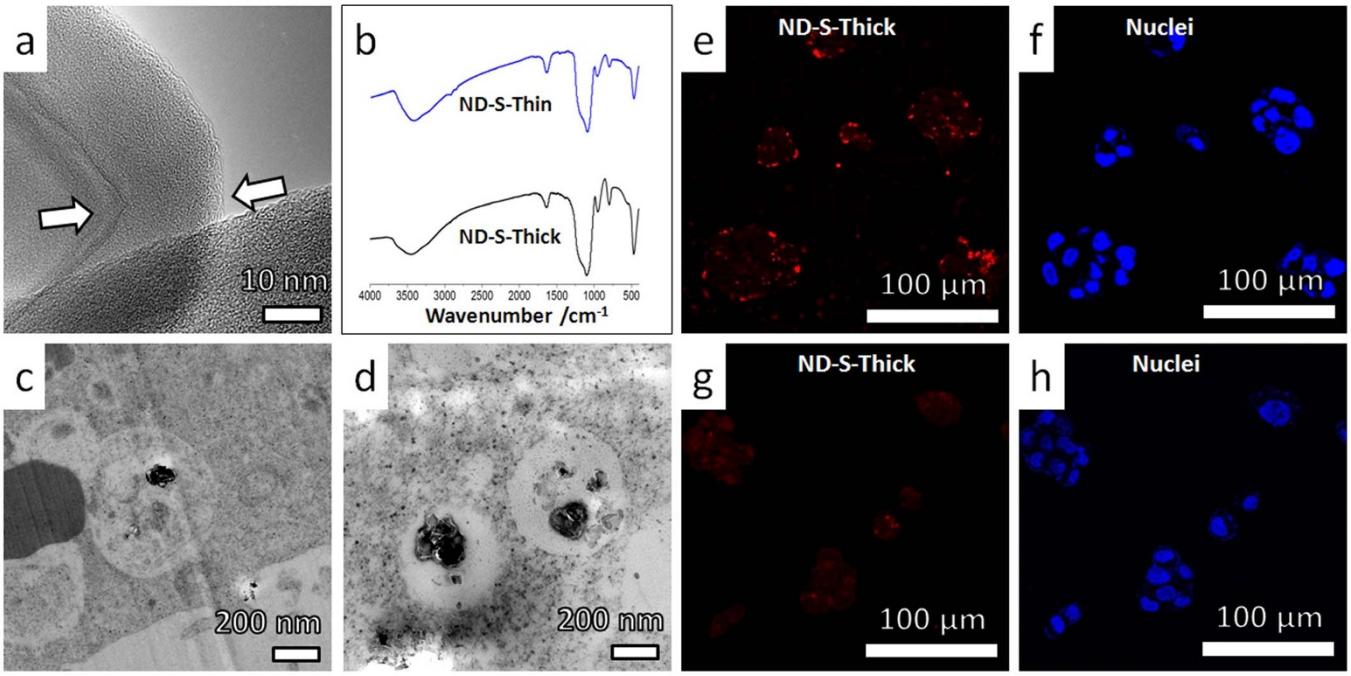

Figure 4 | Intracellular translocation and cellular excretion behaviors of ND-S-Thick particles (nanodiamonds coated with thick layers of SiO_2). The observed cellular dynamics was similar to that of SiO_2 nanoparticles (Supplementary Fig. S12 and Fig. S13). (a) High-resolution TEM image showing a ~15 nm thick silica shell on the surface of ND-S-Thick particles. The sharp corner of the nanodiamonds was rounded up by silica coating. (b) Similarity between FTIR spectra of ND-S-Thick and ND-S-Thin particles indicates that the two kinds of nanoparticles have similar surface chemistry. (c–d) Typical TEM images showing distribution of ND-S-Thick particles in membrane bounded vesicles, in HepG2 cells after incubation in serum-free medium for 24 hours. (e–h) Representative confocal microscopy images showing the uptake and excretion of ND-S-Thick particles in HepG2 cells as revealed by the fluorescence of NDs (red). The nuclei were stained by DAPI (blue). (e,f) HepG2 cells were incubated with ND-S-Thick particles in serum-free medium for 12 hours. Punctated red dots (fluorescent signal from ND-S-Thick) shows effective cellular uptake. (g,h) HepG2 cells were incubated for additional 12 hours in particles-free serum-free medium. Greatly reduced fluorescent signal from the ND-S-Thick (red dots) shows >75% ND-S-Thick particles exited the cells after the "washing" process.

that of SiO_2 (Supplementary Fig. S14 a–e). The FTIR spectrum of the ND-S-thin samples showed that their surface chemistry resembled that of SiO_2 NPs rather than NDs (Fig. 3b). The thin SiO_2 coated NDs had similar zeta potential to that of uncoated NDs at pH ~ 7.6 (Supplementary Fig. S3).

The cellular translocation and excretion characteristics of ND-S-Thin particles were found similar to those of NDs, although their surface chemical composition had been modified to that of SiO_2 NPs. After they entered the cells, ~90% (see Supplementary Table S1) of the ND-S-Thin particles escaped to cytoplasm (with 24 hours' incubation), rather than resided stably in the endosomes (Fig. 3c–e). Similar to NDs, a few ND-S-thin particles were observed in the process of passing through the vesicle membranes (Fig. 3f). Confocal microscopy images (Fig. 3g & h) of the HepG2 cells taken after 12 hours' incubation with the ND-S-Thin particles confirmed the intake of NPs. Decrease in the amount of NPs was unnoticeable when the cells were further incubated in NPs-free medium for another 12 hours (Fig. 3i & j). These results meant that the SiO_2 like surface chemical composition had negligible effects on the cellular fate of the NDs.

To further confirm the morphological effect, we study the cellular dynamics of Sample ND-S-Thick, which were prepared by growing thicker SiO_2 layers on the surfaces of the NDs with the sharp corners of the NDs rounded up. The ND-S-Thick particles had morphological characteristics similar to those of SiO_2 NPs (Supplementary Fig. S1c). Amorphous layers of Si and O with ~15 nm thickness were uniformly formed on the surface of the NDs (Fig. 4a). The surface chemistry remained similar to that of ND-S-thin (Fig. 4b), and the zeta potential (surface charge characteristic) of thickly coated NDs (by SiO_2) was similar to that of the uncoated ND at pH ~ 7.6 (Fig. S3). Also, the average size of the ND-S-Thick particles was only slightly (20%) larger than that of the uncoated NDs. The average hydrodynamic radius of the NPs was measured as ~131 nm (Fig. S2) by DLS, only ~10% larger than that of uncoated NDs. The cellular translocation and excretion behaviors of the ND-S-Thick particles were completely different from those of NDs and ND-S-Thin particles, but resembled those of SiO_2 NPs. More than 90% (see Supplementary Table S1) of the ND-S-Thick particles stably resided in the endosomes/lysosomes upon their cellular intake (Fig. 4c & d). Moreover, the ND-S-Thick particles were found to exit the cells easily: The confocal microscopy images of HepG2 cells incubated with ND-S-Thick particles for 12 hours (Fig. 4e & f) and followed by another 12 hours' incubation in NPs-free medium (Fig. 4g & h) showed the amount of ND-S-Thick particles reduced to <25% after the "wash-out" process.

To further exclude the surface composition effect, we investigated the cellular dynamics of round-shaped ND samples (Fig. 5a), which were obtained by direct chemical etching of the prickly NDs. Such round-shaped NDs had surface chemistry and electrostatics similar to uncoated sharp-shaped NDs (Fig. 5b and Supplementary Fig. S3). Contrary to the case of uncoated prickly NDs, we found stable endosomal residence of the round-shaped NDs (Fig. 5c & d) after their incubation with the respective cells for 24 hours. At the same time, the cellular excretion of the round-shaped ND was found easy, i.e., >85% of the round-shaped NDs were excreted after the "wash-out" process (Fig. 5e–h).

To investigate whether the morphological effect was universal in determining the cellular fate of NPs, we carried out further experiments on a completely different material system, namely, Au nanostructures. The Au nanostructures had very different surface

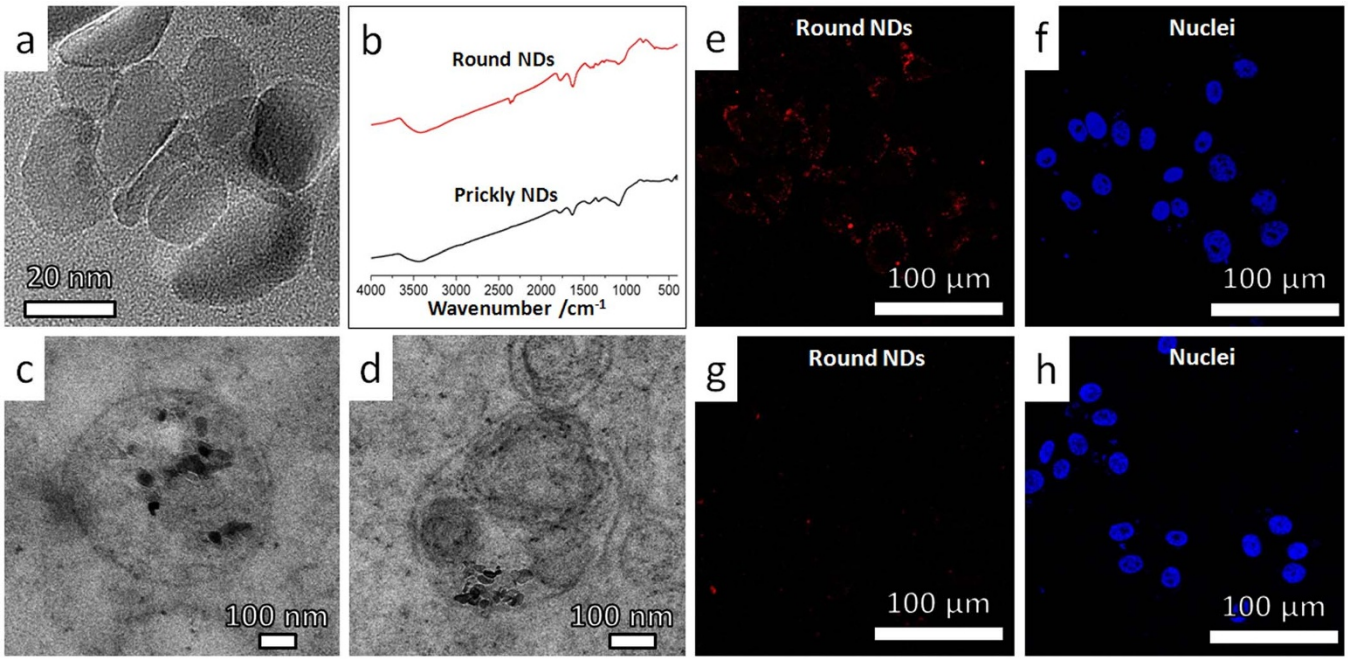

Figure 5 | Intracellular translocation and cellular excretion behaviors of round nanodiamonds. The observed cellular dynamics was similar to that of SiO_2 nanoparticles (Supplementary Fig. S12 and Fig. S13). (a) High-resolution TEM image showing the corners and edges of such nanodiamonds were rounded up as compared with prickly nanodiamonds (Fig. 2a). (b) Similarity between FTIR spectra of round NDs and prickly NDs indicates that the two kinds of nanoparticles have similar surface chemistry. (c–d) Typical TEM images showing distribution of round NDs in membrane bounded vesicles, in HepG2 cells after incubation in serum-free medium for 24 hours. (e–h) Representative confocal microscopy images showing the uptake and excretion of round NDs in HepG2 cells as revealed by the fluorescence of NDs (red). The nuclei were stained by DAPI (blue). (e,f) HepG2 cells were incubated with round NDs in serum-free medium for 12 hours. Punctated red dots (fluorescent signal from ND-S-Thick) shows effective cellular uptake. (g,h) HepG2 cells were incubated for additional 12 hours in particles-free serum-free medium. Greatly reduced fluorescent signal from the round NDs (red dots) shows >85% round NDs exited the cells after the "washing" process.

chemistry and charge characteristics from those of NDs or SiO_2. The surfaces of the Au nanostructures were modified by polyethylene glycol (PEG), leading to methoxy group dominated surface chemistry. The FTIR spectra (Fig. 6a) presented peaks at 2920 cm^{-1}, 2850 cm^{-1} and 1114 cm^{-1}, which are characteristic of PEG, confirming the successful immobilization of the PEG chains at the Au nanostructures' surface. The surfaces of the Au nanostructures were nearly neutral, with measured zeta potential ~0 mV (Supplementary Fig. S15).

Two different morphologies of the Au nanostructures were selected for further experiments, namely, spherical Au nanospheres of ~150 nm diameter (Fig. 6b) and prickly Au nanostars ~150 nm size (Fig. 6d). After HepG2 cells being incubated with two respective Au NPs for 24 hours, a majority (~90%, see Supplementary Table S1) of the Au nanospheres were found in membrane bounded vesicles (Fig. 6c), while most (~95%, see Supplementary Table S1) of the Au nanostars were located in the cytoplasm (Fig. 6e). Consistently, cellular excretion of the Au nanospheres was found to be easy, while that of the Au nanostars was difficult (Supplementary Fig. S16).

Discussion

The main results of this paper are summarized in Table 1. It is unambiguously demonstrated that the morphological features of the NPs played a dominant role in determining the NPs' cellular translocation and in turn their excretion. On the contrary, the surface chemical and electrostatic properties and the chemical compositions of the nanoparticles are not important factors.

The present experimental results suggested the size of NPs in determining their intracellular translocation (after endocytosis) was not obvious. First, the uncoated, thin SiO_2 coated and thick SiO_2 coated ND samples have similar average hydrodynamic radii while the NDs with different morphological features had dramatically different intracellular distributions. Second, the two types of Au NPs had similar hydrodynamic radii but totally different cellular dynamics. Finally, our examination on ND samples of smaller physical sizes (with average hydrodynamic radius measured as ~35 nm) showed similar intracellular distribution to the larger sized NDs (Supplementary Fig. S17).

To quantify the degree of NPs' sharpness, we adopted the circularity (roundness), defined by its projected cross sectional area A and perimeter P as $C = 4A\pi/(P^2)$[37]. We used high resolution TEM to measure the geometrical parameters of the NPs. By randomly choosing one hundred particles from each type of sample, we obtained the distribution of NPs' circularity for all six samples (Supplementary Fig. S18 a–f). The average circularity for all samples was listed in Table S1 in Supporting Information. The NDs (average circularity ~0.556) and ND-S-Thin (average circularity ~0.571) had the highest degree of sharpness among the NDs-based samples (ND-S-Thick average circularity ~0.867, round-shaped ND average circularity ~0.780). Consistently, Au nanostars (average circularity ~0.351) also showed a much higher degree of sharpness when compared to Au nanospheres (average circularity ~0.931). Considering all the samples investigated in the present study, those with average circularity <0.6 were consistently found to reside in cytoplasm (>90%) after cellular uptake, while those with higher average circularity values (e.g. >0.78) preferred to reside in endosome or lysosome compartments (~10% in cytoplasm). Therefore, the observed endosomal release of the NPs was a result of their high sharpness.

Recently, some theoretical works[38,39] suggested the NPs' shape as a critical factor in determining the translocation of NPs across a lipid bilayer, although the modeling there was for different scenarios ("cutting through" under an external driving force[39] or by switching the NPs' surface between hydrophobicity and hydrophilicity[38]). Obviously, the "spontaneous penetration" observed in the present

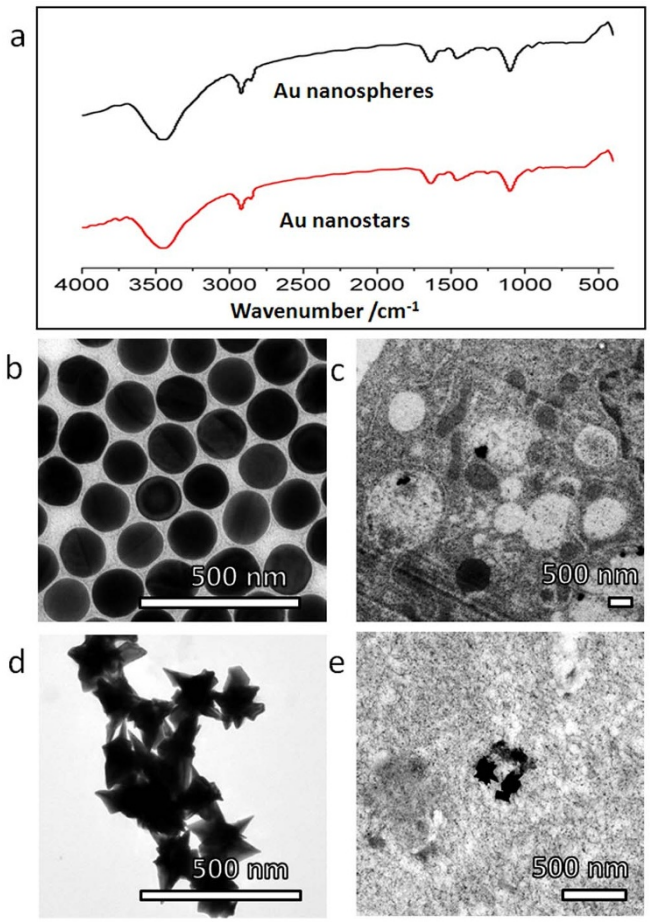

Figure 6 | Different intracellular translocation behaviors between Au nanospheres (low sharpness) and nanostars (high sharpness). (a) Identical features in the FTIR spectra of Au nanospheres and Au nanostars indicate that they have similar surface chemistry. (b) TEM image of Au nanospheres. (c) Typical TEM images showing stable residence of Au nanospheres in membrane bounded vesicles, in HepG2 cells after incubation in serum-free medium for 24 hours. (d) TEM image of Au nanostars. (e) Typical TEM images showing distribution of Au nanostars in cytoplasm, in HepG2 cells after incubation in serum-free medium for 24 hours.

study did not involve any external driving force. It did not involve any hydrophobicity and hydrophilicity switching either. While further study is still needed to fully understand the driving force of the penetration through vesicle membranes by the sharp-shaped NPs, the experimental results are consistent with the simulation[38,39] in that the penetration efficiency increased with the decrease of the contact area or increase of NP's local curvature at the contact point.

It should be noted that the sharp-shaped NPs were not observed to directly penetrate the plasma membranes while they could penetrate the endosomal membranes easily. Such difference may be explained by the differences between the plasma membranes and the endosomal membranes, including composition and curvature. Although the endosomal membranes are derived from the plasma membrane, a lot of modification in the lipid content of the endosomal membranes occurs throughout the formation process of the endosome[40,41]. In particular, there is a decrease in sterol, phosphatidylserine, sphingolipid (the presence of which strengthen the lipid membrane), and increase in bis(monoacylglycero)phosphate (which creates strain in a membrane and facilitates easy particle insertion) in the endosomal membrane as compared with the plasma membrane. Consequently, it is possible that the endosomal membrane is more volatile to be damaged by NPs. On the other hand, the radius curvature of membrane may also play a role in its mechanical stability[38].

Methods

Preparation of NPs. The NDs were obtained by high pressure high temperature (HPHT) method[44]. The ND-S-Thin and ND-S-Thick particles were prepared by growing an amorphous silica layer onto the NDs[42,45,46]. 1 ml aqueous as-received NDs (1 mg/ml) particles were mixed with 10 μl (3-Aminopropyl)triethoxysilane (APTES) (Sigma) under stirring for 2 hours at room temperature. After that the NDs were separated by centrifugation. For ND-S-Thin particles, 3.75 ml NDs-APTES particles (in ethanol) were mixed with 1.15 ml deionized H_2O and 75 μl 30% ammonia-water solution, before 5 μl Tetraethyl orthosilicate (TEOS) (Sigma) was added. The mixture was stirred for 0.5 hour at room temperature and then the ND-S-Thin particles were obtained by centrifugation. For ND-S-Thick particles, 3.75 ml NDs-APTES particles (in ethanol) were mixed with 1.15 ml deionized H_2O and 90 μl 30% ammonia-water solution, before 10 μl TEOS was added. The mixture was stirred for 2 hours at room temperature and then the ND-S-Thick particles were obtained by centrifugation. Centrifugation was applied to obtain the NDs with smaller or larger physical size. Round-shaped NDs were produced by short-term oxidation of prickly NDs in melted potassium nitrate[43]. Briefly, the prickly HPHT ND powder (Microdiamant, MSY 0–0.05) was heated with KNO_3 (1 : 200 w:w) at 535°C for 8 minutes. The quickly cooled meltage was dissolved in water, centrifuged, treated with concentrated HF for 1 hour at 50°C and centrifuged. The surface chemistries of the round-shaped NDs were normalized according to common procedures[47]. The amorphous silica NPs were synthesized using the modified Stober's method, which produced spherical NPs with controllable size and narrow size distribution. The spherical and star shaped Au NPs were synthesized using the seed mediated method. After that, the as-synthesized spherical Au NPs were oxidized to obtain smooth surface[48]. Then these Au NPs were pegylated by mixing them with freshly prepared aqueous mPEG-SH solution (1 mM, 2 ml; NANOCS, America) in 30°C water bath overnight.

Characterization of NPs. The morphology and size of the NPs were characterized using low magnification transmission electron microscopy (TEM, PhilipsCM120). The detailed morphological feature of NPs was investigated using high resolution TEM (Tecnai G2, FEG). The photoluminescence of NDs, ND-S-Thin and ND-S-Thick particles was obtained on a home-built fluorescence spectrometer equipped with a continuous-wave 514 nm laser[49]. The surface of NPs was studied by Fourier Transform Infrared Spectrometer (FTIR; Nicolet 670, Thomas Nicolet, Waltham, MA). The surface composition of ND-S-Thin and ND-S-Thick particles was investigated by X-ray Photoelectron Spectrometer (XPS) (PHI Quantum 2000). The average zeta potential of NPs in PBS buffer solution was measured using a commercial zeta potential spectrometer (ZetaPlus, Brookhaven). The size distribution of NDs, ND-S-Thin and ND-S-Thick particles in PBS buffer solution were measured using dynamic light scattering (DLS) at an angle of 20°. The apparatus used for DLS measurements was an ALV-5000 goniometer (ALV Laser) equipped with a helium–neon laser and a digital correlator. All measurements were carried out at room temperature (25°C). The distribution of circularity of NPs was semi-quantitatively obtained by using TEM to examine their corresponding geometrical parameters on one hundred randomly chosen particles from each sample. The average circularity was obtained by Gaussian fitting of the above data.

Table 1 | Summary of intracellular trafficking and cellular excretion of nanoparticles with various chemical compositions, shapes, and surfaces. The sharp-shaped nanoparticles, regardless of their surfaces and chemical compositions, have high probability of translocation into cytoplasm through piercing the endosomes and low probability of cellular excretion. The case is opposite for the round-shaped nanoparticles

	Translocation from endosomes to cytoplasm		Cellular excretion	
Material systems	Sharp shaped	Round shaped	Sharp shaped	Round shaped
Uncoated nanodiamonds	Yes	No	Difficult	Easy
SiO_2 coated nanodiamonds	Yes	No	Difficult	Easy
Au nanoparticles	Yes	No	Difficult	Easy

Introducing NPs to cells. The human liver carcinoma HepG2 cell line, the human colon cancer HCT116 cell line and the human breast cancer LCC6 cell line were used in this study. The HepG2 cells and LCC6 cells were cultured in Dulbecco's modified Eagle's medium (DMEM, Gibco), supplemented with 10% heat-inactivated Fetal bovine serum (FBS), 2.0 g/L sodium bicarbonate, 0.1 g/L streptomycin sulfate, 0.06 g/L penicillin G and 5.958 g/L HEPES. The HCT116 cells were cultured in RPMI 1640 medium (Gibco) with same concentrations of FBS and antibiotics. The cells were maintained in a standard cell culture incubator at 37°C in a humidified atmosphere with 5% CO_2. All of the NPs were sterilized by steaming at 115°C (NPs in powder form) for 2 hours, before they were dispersed in the medium and introduced to the cells, which had already been seeded and incubated for 24 hours. The feeding concentration of the NPs was always kept at 10 μg/ml unless otherwise specified. Different cell feeding durations were adopted, as specified in the corresponding result description.

Characterizations of cells. For TEM study, the NP-fed cells were fixed using typical procedures published elsewhere[35] at the end of their incubation with NPs. Microtome (Leica, EM UC6) was used to cut the cured cell cube (in Spurr resin (Electron microscopy sciences, USA)) into thin slices (70–90 nm in thickness). The samples were then collected on 300-mesh copper grids and double stained with 2% aqueous uranyl acetate and commercial lead citrate aqueous solution (Leica). For each of the sample in the present study, the TEM study has been carried out on many different NPs in several tens of cell samples. For all confocal microscopy studies, the NP-fed cells were fixed with 4% paraformaldehyde at room temperature, before their being observed using confocal laser scanning microscopy (TCSP5, Leica) with a 63× water-immersion objective lens. For all dark field microscopy studies, the NP-fed cells were fixed with 4% paraformaldehyde at room temperature, before their being observed using the home-built light microscope[49].

The cellular uptake pathway of NDs was investigated by pretreating cells with inhibitor NaN_3 (10 mM, Sigma) or at 4°C for 3 hours in serum-free medium. After that, the original medium was discarded and the cells were further treated with NDs for 6 hours in serum-free medium. At the end of the incubation, the cells were washed with PBS, fixed with 70% ethanol, and then processed for flow-cytometry (FACScan, Becton Dickinson, Canada) analysis. The intracellular localization of NDs was investigated by immunofluorescence, i.e., the endosome marker (C10586, Invitrogen) for endosome study, and LysoTracker (L7526, Invitrogen) for lysosome study according to the manufacturer's instructions. The excretion of Au nanostructures was investigated by dark field microscopy. The real time multiple particle tracking technique[33] was adopted to study the movement of NDs inside cells after 24 hours' incubation. By manually focusing on one selected cell within certain periods under confocal microscope, the red bright spots (fluorescence of NDs) were monitored and recorded. The obtained confocal microscopy images were then analyzed by ImageJ (National Institutes of Health, USA). The intracellular distributions of various nanostructures after their 24 hours' incubation in serum-free medium were obtained by randomly choosing a number of cells and analyzing >100 TEM images for each sample. The TEM grid squares were first briefly imaged and marked to prevent repetitive imaging. Next, the whole cells in the grid squares were imaged at lower magnification. Each cell was scanned for areas of NPs, which were identified by their diffractions (for crystalline samples) and energy dispersive X-ray (EDX) spectroscopy (for non-carbon samples). These areas were further imaged at high magnification to allow identification of nanostructures' specific locations.

1. Wang, X. *et al.* Pluronic F108 Coating Decreases the Lung Fibrosis Potential of Multiwall Carbon Nanotubes by Reducing Lysosomal Injury. *Nano Lett.* **12**, 3050–3061 (2012).
2. Meng, L. *et al.* Short Multiwall Carbon Nanotubes Promote Neuronal Differentiation of PC12 Cells via Up-Regulation of the Neurotrophin Signaling Pathway. *Small* **9**, 1786–1798 (2013).
3. Meng, H. *et al.* Engineered Design of Mesoporous Silica Nanoparticles to Deliver Doxorubicin and P-Glycoprotein siRNA to Overcome Drug Resistance in a Cancer Cell Line. *ACS Nano* **4**, 4539–4550 (2010).
4. Zhang, X. Q. *et al.* Interactions of nanomaterials and biological systems: Implications to personalized nanomedicine. *Adv. Drug Deliv. Rev.* **64**, 1363–1384 (2012).
5. Slowing, I. I., Vivero-Escoto, J. L., Wu, C. W. & Lin, V. S. Y. Mesoporous silica nanoparticles as controlled release drug delivery and gene transfection carriers. *Adv. Drug Deliv. Rev.* **60**, 1278–1288 (2008).
6. Panyam, J. & Labhasetwar, V. Biodegradable nanoparticles for drug and gene delivery to cells and tissue. *Adv. Drug Deliv. Rev.* **64**, 61–71 (2012).
7. Fang, C.-Y. *et al.* The Exocytosis of Fluorescent Nanodiamond and Its Use as a Long-Term Cell Tracker. *Small* **7**, 3363–3370 (2011).
8. Vaijayanthimala, V. *et al.* The long-term stability and biocompatibility of fluorescent nanodiamond as an in vivo contrast agent. *Biomaterials* **33**, 7794–7802 (2012).
9. McGuinness, L. P. *et al.* Quantum measurement and orientation tracking of fluorescent nanodiamonds inside living cells. *Nat. Nanotechnol.* **6**, 358–363 (2011).
10. Kucsko, G. *et al.* Nanometre-scale thermometry in a living cell. *Nature* **500**, 54–58 (2013).
11. Sahay, G., Alakhova, D. Y. & Kabanov, A. V. Endocytosis of nanomedicines. *J. Control. Release* **145**, 182–195 (2010).
12. Wieffer, M., Maritzen, T. & Haucke, V. SnapShot: Endocytic Trafficking. *Cell* **137**, 382.e1–382.e3 (2009).
13. Grant, B. D. & Donaldson, J. G. Pathways and mechanisms of endocytic recycling. *Nat. Rev. Mol. Cell Biol.* **10**, 597–608 (2009).
14. Zhao, F. *et al.* Cellular Uptake, Intracellular Trafficking, and Cytotoxicity of Nanomaterials. *Small* **7**, 1322–1337 (2011).
15. Chithrani, B. D. & Chan, W. C. W. Elucidating the mechanism of cellular uptake and removal of protein-coated gold nanoparticles of different sizes and shapes. *Nano Lett.* **7**, 1542–1550 (2007).
16. Fader, C. M. & Colombo, M. I. Autophagy and multivesicular bodies: two closely related partners. *Cell Death and Differ.* **16**, 70–78 (2009).
17. Khalil, I. A., Kogure, K., Akita, H. & Harashima, H. Uptake pathways and subsequent intracellular trafficking in nonviral gene delivery. *Pharmacol Rev.* **58**, 32–45 (2006).
18. Ghosh, P. S., Kim, C. K., Han, G., Forbes, N. S. & Rotello, V. M. Efficient Gene Delivery Vectors by Tuning the Surface Charge Density of Amino Acid-Functionalized Gold Nanoparticles. *ACS Nano* **2**, 2213–2218 (2008).
19. Gilleron, J. *et al.* Image-based analysis of lipid nanoparticle-mediated siRNA delivery, intracellular trafficking and endosomal escape. *Nat. Biotechnol.* **31**, 638–646 (2013).
20. Slowing, I. I., Trewyn, B. G. & Lin, V. S. Y. Mesoporous silica nanoparticles for intracellular delivery of membrane-impermeable proteins. *J. Am. Chem. Soc.* **129**, 8845–8849 (2007).
21. Wang, L. *et al.* Selective Targeting of Gold Nanorods at the Mitochondria of Cancer Cells: Implications for Cancer Therapy. *Nano Lett.* **11**, 772–780 (2011).
22. Li, W. *et al.* The translocation of fullerenic nanoparticles into lysosome via the pathway of clathrin-mediated endocytosis. *Nanotechnology* **19**, 145102 (2008).
23. Lao, F. *et al.* Fullerene Nanoparticles Selectively Enter Oxidation-Damaged Cerebral Microvessel Endothelial Cells and Inhibit JNK-Related Apoptosis. *ACS Nano* **3**, 3358–3368 (2009).
24. Dobrovolskaia, M. A. & McNeil, S. E. Immunological properties of engineered nanomaterials. *Nat. Nanotechnol.* **2**, 469–478 (2007).
25. Vonarbourg, A., Passirani, C., Saulnier, P. & Benoit, J. P. Parameters influencing the stealthiness of colloidal drug delivery systems. *Biomaterials* **27**, 4356–4373 (2006).
26. Panyam, J., Zhou, W. Z., Prabha, S., Sahoo, S. K. & Labhasetwar, V. Rapid endo-lysosomal escape of poly(DL-lactide-co-glycolide) nanoparticles: implications for drug and gene delivery. *FASEB J.* **16**, 1217–1225 (2002).
27. Guo, S. *et al.* Enhanced Gene Delivery and siRNA Silencing by Gold Nanoparticles Coated with Charge-Reversal Polyelectrolyte. *ACS Nano* **4**, 5505–5511 (2010).
28. Ji, Z. *et al.* Designed Synthesis of CeO2 Nanorods and Nanowires for Studying Toxicological Effects of High Aspect Ratio Nanomaterials. *ACS Nano* **6**, 5366–5380 (2012).
29. Tu, Y. S. *et al.* Destructive extraction of phospholipids from Escherichia coli membranes by graphene nanosheets. *Nat. Nanotechnol.* **8**, 594–601 (2013).
30. Yanes, R. E. *et al.* Involvement of Lysosomal Exocytosis in the Excretion of Mesoporous Silica Nanoparticles and Enhancement of the Drug Delivery Effect by Exocytosis Inhibition. *Small* **9**, 697–704 (2013).
31. Chung, P. H., Perevedentseva, E., Tu, J. S., Chang, C. C. & Cheng, C. L. Spectroscopic study of bio-functionalized nanodiamonds. *Diamond and Related Materials* **15**, 622–625 (2006).
32. Panyam, J. & Labhasetwar, V. Dynamics of endocytosis and exocytosis of poly(D,L-lactide-co-glycolide) nanoparticles in vascular smooth muscle cells. *Pharm. Res.* **20**, 212–220 (2003).
33. Suh, J., Dawson, M. & Hanes, J. Real-time multiple-particle tracking: applications to drug and gene delivery. *Adv. Drug Deliv. Rev.* **57**, 63–78 (2005).
34. Nan, X. L., Sims, P. A., Chen, P. & Xie, X. S. Observation of individual microtubule motor steps in living cells with endocytosed quantum dots. *J. Phys. Chem. B* **109**, 24220–24224 (2005).
35. Chu, Z., Huang, Y., Tao, Q. & Li, Q. Cellular uptake, evolution, and excretion of silica nanoparticles in human cells. *Nanoscale* **3**, 3291–3299 (2011).
36. Chu, Z., Huang, Y., Lib, L., Tao, Q. & Li, Q. Physiological pathway of human cell damage induced by genotoxic crystalline silica nanoparticles. *Biomaterials* **33**, 7540–7546 (2012).
37. Hentschel, M. L. & Page, N. W. Selection of descriptors for particle shape characterization. *Part. Part. Syst. Char.* **20**, 25–38 (2003).
38. Ding, H. M., Tian, W. D. & Ma, Y. Q. Designing Nanoparticle Translocation through Membranes by Computer Simulations. *ACS Nano* **6**, 1230–1238 (2012).
39. Yang, K. & Ma, Y.-Q. Computer simulation of the translocation of nanoparticles with different shapes across a lipid bilayer. *Nat. Nanotechnol.* **5**, 579–583 (2010).
40. van Meer, G., Voelker, D. R. & Feigenson, G. W. Membrane lipids: where they are and how they behave. *Nat. Rev. Mol. Cell Biol.* **9**, 112–124 (2008).
41. McMahon, H. T. & Gallop, J. L. Membrane curvature and mechanisms of dynamic cell membrane remodelling. *Nature* **438**, 590–596 (2005).
42. Weng, M.-F., Chang, B.-J., Chiang, S.-Y., Wang, N.-S. & Niu, H. Cellular uptake and phototoxicity of surface-modified fluorescent nanodiamonds. *Diamond and Related Materials* **22**, 96–104 (2012).
43. Havlik, J. *et al.* Boosting nanodiamond fluorescence: towards development of brighter probes. *Nanoscale* **5**, 3208–3211 (2013).
44. Chang, Y.-R. *et al.* Mass production and dynamic imaging of fluorescent nanodiamonds. *Nat. Nanotechnol.* **3**, 284–288 (2008).

45. Rehor, I. *et al*. Fluorescent Nanodiamonds Embedded in Biocompatible Translucent Shells. *Small*, 10.1002/smll.201302336 (2013).
46. Rehor, I. *et al*. Fluorescent nanodiamonds with bioorthogonally reactive protein-resistant polymeric coatings. *ChemPlusChem* **79**, 21–24 (2014).
47. Fu, C. C. *et al*. Characterization and application of single fluorescent nanodiamonds as cellular biomarkers. *Proc. Natl. Acad. Sci. USA*. **104**, 727–732 (2007).
48. Rodriguez-Fernandez, J., Perez-Juste, J., Mulvaney, P. & Liz-Marzan, L. M. Spatially-directed oxidation of gold nanoparticles by Au(III)-CTAB complexes. *J. Phys. Chem. B* **109**, 14257–14261 (2005).
49. Xiao, M., Chen, H., Ming, T., Shao, L. & Wang, J. Plasmon-Modulated Light Scattering from Gold Nanocrystal-Decorated Hollow Mesoporous Silica Microspheres. *ACS Nano* **4**, 6565–6572 (2010).

Acknowledgments

We thank JF Wang's group for providing the Au nanosphere samples. This work was supported by CRF of RGC (Project No. CUHK4/CRF/12G), and the National Basic Research Program of China (973 Program) under Grant No. 2014CB921402. P.C. and I.R. were supported by grants of GACR (Project P108/12/0640) and MSMT CR (Grant No. LH11027).

Author contributions

Z.Q.C. and Q.L. designed the project. Z.Q.C., S.L.Z., B.K.Z. and C.Y.Z. carried out the experiments. C.Y.F. and H.C.C. provided the prickly nanodiamonds. I.R. and P.C. provided the round nanodiamonds. G.L. supervised all the in vitro experiment. Q.L., R.-B.L. and Z.Q.C. wrote the paper. All authors analyzed the data and discussed on the manuscript.

Additional information

Supplementary information accompanies this paper at http://www.nature.com/scientificreports

Competing financial interests: The authors declare no competing financial interests.

How to cite this article: Chu, Z.Q. *et al.* Unambiguous observation of shape effects on cellular fate of nanoparticles. *Sci. Rep.* **4**, 4495; DOI:10.1038/srep04495 (2014).